Front. Mech. Eng. 2018, 13(1): 48–52
https://doi.org/10.1007/s11465-018-0493-y

RESEARCH ARTICLE

Jiehua LI, Bernd OBERDORFER, Daniel HABE, Peter SCHUMACHER

Determining casting defects in near-net shape casting aluminum parts by computed tomography

© Higher Education Press and Springer-Verlag GmbH Germany, part of Springer Nature 2018

Abstract Three types of near-net shape casting aluminum parts were investigated by computed tomography to determine casting defects and evaluate quality. The first, second, and third parts were produced by low-pressure die casting (Al-12Si-0.8Cu-0.5Fe-0.9Mg-0.7Ni-0.2Zn alloy), die casting (A356, Al-7Si-0.3Mg), and semi-solid casting (A356, Al-7Si-0.3Mg), respectively. Unlike die casting (second part), low-pressure die casting (first part) significantly reduced the formation of casting defects (i.e., porosity) due to its smooth filling and solidification under pressure. No significant casting defect was observed in the third part, and this absence of defects indicates that semi-solid casting could produce high-quality near-net shape casting aluminum parts. Moreover, casting defects were mostly distributed along the eutectic grain boundaries. This finding reveals that refinement of eutectic grains is necessary to optimize the distribution of casting defects and reduce their size. This investigation demonstrated that computed tomography is an efficient method to determine casting defects in near-net shape casting aluminum parts.

Keywords near-net shape casting, aluminum parts, casting defects, low pressure die casting, die casting, semi-solid casting, computed tomography

1 Introduction

High-performance Al alloys are widely used to replace heavy cast iron and steel parts in automotive and defense industries due to their small weight, high specific strength, and good corrosive resistance. Near-net shape casting of Al parts (i.e., direct chill casting, low-pressure die casting (LPDC), and semi-solid casting (SSC)) is promising because the shape and properties of the parts can be controlled by near-net shape casting technologies; therefore, subsequent manufacturing processes are not required. For example, direct chill casting of near-net shape ingots has been performed to produce suspension parts of Al alloys without extrusion and bending procedures [1]. In terms of shape casting, LPDC has been used to produce large, complex, thin-walled, high-quality Al casting parts [2–5]. LPDC is a counter-gravity casting (CGC) technology. Other CGC approaches include counter-pressure casting and vacuum-assisted pressure-adjusted casting. Casting in CGC is formed under pressure. Therefore, primary and secondary dendrites are broken and distributed evenly within the matrix, thus improving the performance of castings. LPDC presents many advantages over other commercial methods due to its smooth filling and solidification under pressure. The formation of casting defects (i.e., pore and/or shrinkage cavities) can be significantly reduced. However, appropriate technology parameters have to be provided; otherwise, these inherent advantages cannot be maximized. SSC has also been used to produce high-quality Al casting parts. Primary and secondary dendrites are broken in SSC, and round grains are formed. Therefore, the formation of casting defects is also significantly reduced. Computed tomography (CT) is frequently utilized to determine the casting defects of Al casting parts [6–11]. This study determines casting defects and evaluates the quality of three types of near-net shape casting aluminum parts by using CT.

Received March 27, 2017; accepted September 27, 2017

Jiehua LI (✉), Peter SCHUMACHER
Institute of Casting Research, Montanuniversität Leoben, Leoben A-8700, Austria
E-mail: jie-hua.li@hotmail.com

Bernd OBERDORFER, Daniel HABE, Peter SCHUMACHER
Austrian Foundry Research Institute, Leoben A-8700, Austria

2 Experimental

Three types of near-net shape casting aluminum parts were investigated by CT to determine casting defects and evaluate quality. The first, second, and third parts were produced by die casting (A356, Al-7Si-0.3Mg), LPDC

(Al-12Si-0.8Cu-0.5Fe-0.9Mg-0.7Ni-0.2Zn alloy), and SSC (A356, Al-7Si-0.3Mg), respectively. Although different Al alloys and casting technologies were used, the obtained results can still be compared qualitatively.

The samples for CT investigations were machined to obtain a 4 mm diameter and 10 mm length. The samples were scanned on a Phoenix X-ray v|tome|x c equipped with a 240 kV cone-beam X-ray tube operating at 70 kV. A total of 1300 X-ray images were recorded within a total scan time of about 120 min by using a GE DXR 1000 × 1000 pixel detector with a 14-bit dynamic range. A modified Feldkamp algorithm for filtered back projection was used for volume reconstruction according to the supplier's instructions [6]. The resulting voxel size was about 5 μm. The number density and size distribution of porosities were determined with three types of near-net shape casting aluminum parts.

3 Results and discussion

Figure 1 shows a 3D image of porosities and a quantitative analysis of porosities of the first part produced by LPDC (Al-12Si-0.8Cu-0.5Fe-0.9Mg-0.7Ni-0.2Zn alloy) (Figs. 1(a) and 1(c)) and the second part produced by die casting (A356, Al-7Si-0.3Mg) (Figs. 1(b) and 1(d)). As shown in Fig. 1(a), porosities with a low number density were observed in the first part produced by LPDC (Al-12Si-0.8Cu-0.5Fe-0.9Mg-0.7Ni-0.2Zn alloy). Large porosities with a high number density were observed in the second part produced by die casting (A356, Al-7Si-0.3Mg), as shown in Fig. 1(b). Given the absence of significant contrast among Al, Si, and Mg, determining the grain boundaries and the position of porosities in the second part is impossible. However, the enhanced contrast caused by the alloying elements (i.e., Cu and Ni) along the grain boundaries in the first part allowed for the determination of the grain boundaries and position of porosities. The casting defects were mostly distributed along the eutectic grain boundaries, indicating that refinement of eutectic grains is necessary to optimize the distribution of casting defects and reduce their size. A quantitative analysis of porosities is also shown in Figs. 1(c) and 1(d). The total volume of porosities in the second part was approximately 1.14%, and the number density of porosities was approximately 26.7 mm^{-3}. By contrast, the total volume of porosities in the first part was 0.05%, which is much less than that (1.14%) of the second part. The number density of porosities was 22.9 mm^{-3}, which is also slightly less than that (26.7 mm^{-3}) of the second part. LPDC significantly reduced the formation of casting defects (i.e., porosity) due to its smooth filling and

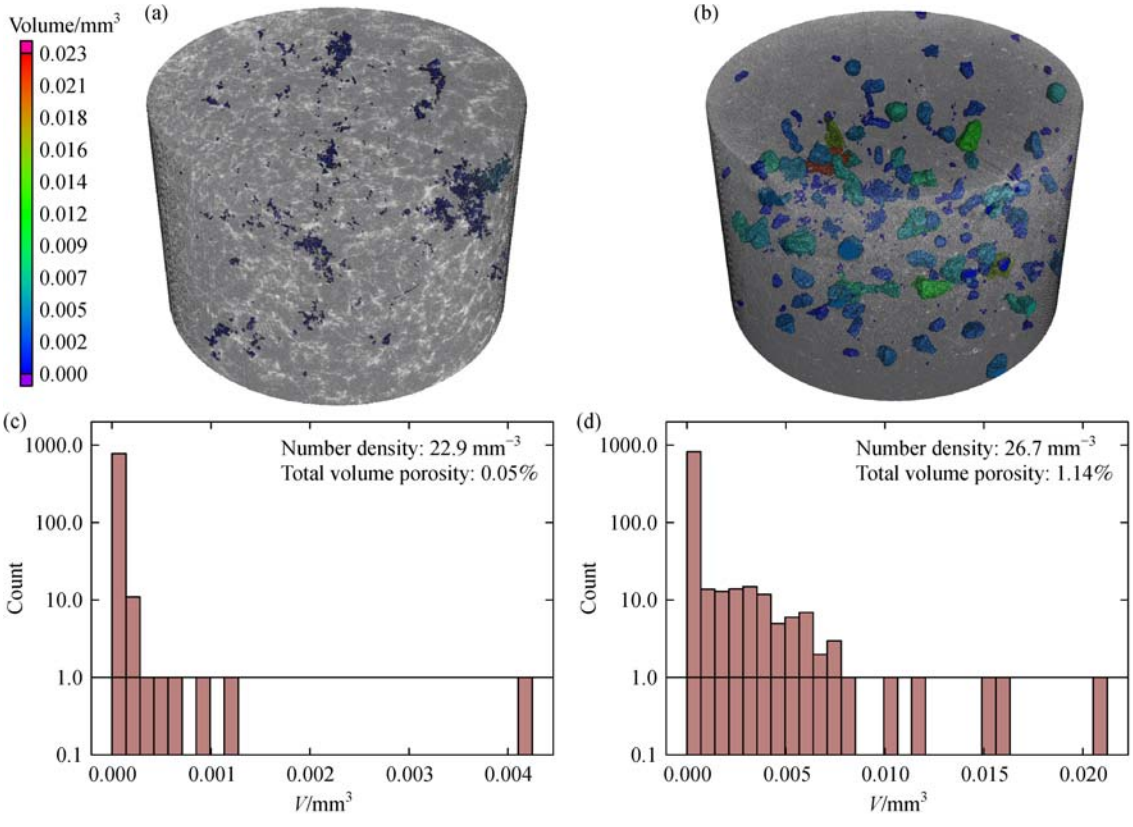

Fig. 1 3D image of porosities and a quantitative analysis of porosities in (a, c) the first part produced by low-pressure die casting (Al-12Si-0.8Cu-0.5Fe-0.9Mg-0.7Ni-0.2Zn alloy) and (b, d) in the second part produced by die casting (A356, Al-7Si-0.3Mg)

solidification under pressure. However, alloy composition may also exert a significant effect on the formation of porosities. A systematic investigation of the formation of porosities under the same solidification conditions is required. The present investigation indicates that CT is an efficient method to determine casting defects in near-net shape casting aluminum parts.

Figure 2 shows optical microscopy images of the first part produced by LPDC (Al-12Si-0.8Cu-0.5Fe-0.9Mg-0.7Ni-0.2Zn alloy) (Fig. 2(a)) and the second part produced by die casting (A356, Al-7Si-0.3Mg) (Fig. 2(b)). In the first part (Fig. 2(a)), different types of intermetallic phases (eutectic Si, π-AlSiMgFe phase, Fe-rich phase, Cu-rich phase, and Ni-phase) were observed along the eutectic grain boundaries. Hence, eutectic grain sizes were easily determined by using a modified Murakami reagent to etch out the eutectic grain boundaries. The total volume of intermetallic phases (eutectic Si, π-AlSiMgFe phase, and Fe-rich phase) in the second part was much less than that in the first part. Therefore, the eutectic grain boundaries showed no contrast even with the modified Murakami reagent. Different types of intermetallic phases can be determined through scanning electron microscope (SEM) and energy-dispersive X-ray spectroscopy (EDS) analyses (not shown here) and can be predicted using Thermo-Calc with the database of TCAl3. To provide an example, we predicted the presence of different types of intermetallic phases, as shown in Fig. 3. The elongation of the first part was less than that of the

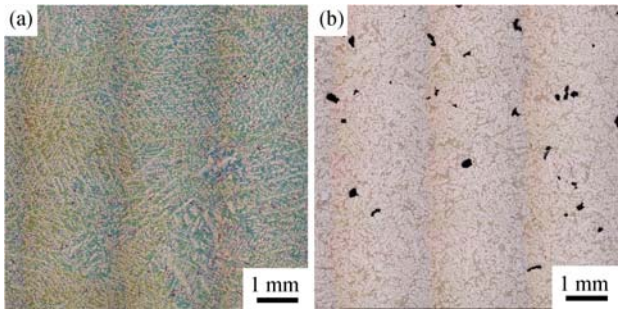

Fig. 2 Optical microscopy images of (a) the first part produced by low-pressure die casting (Al-12Si-0.8Cu-0.5Fe-0.9Mg-0.7Ni-0.2Zn alloy) and (b) the second part produced by die casting (A356, Al-7Si-0.3Mg)

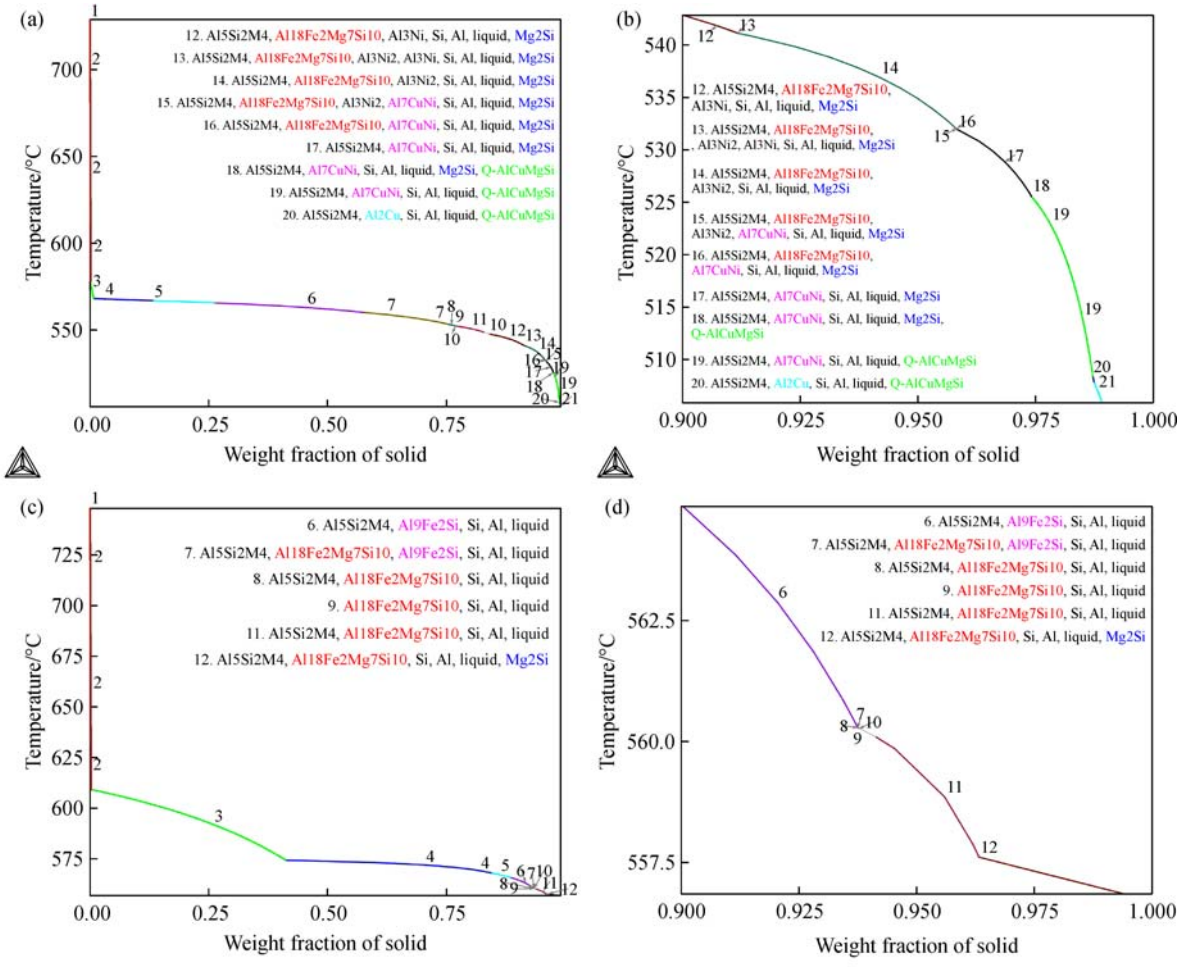

Fig. 3 Solidification path prediction of (a,b) the first part produced by low-pressure die casting (Al-12Si-0.8Cu-0.5Fe-0.9Mg-0.7Ni-0.2Zn alloy) and (b,d) the second part produced by die casting (A356, Al-7Si-0.3Mg); (b,d) is an enlargement of (a,c)

second part, as shown in Fig. 4, due to the presence of different types of intermetallic phases along the grain boundaries. Notably, the presence of different types of intermetallic phases along the grain boundaries increased thermal stability and yield strength at elevated temperatures because Ni- and Cu-containing phases formed in the last stage of solidification, as shown in Fig. 3. They were located in the vicinity of the network of eutectic Si and thus provided a significant contribution to yield strength at elevated temperatures.

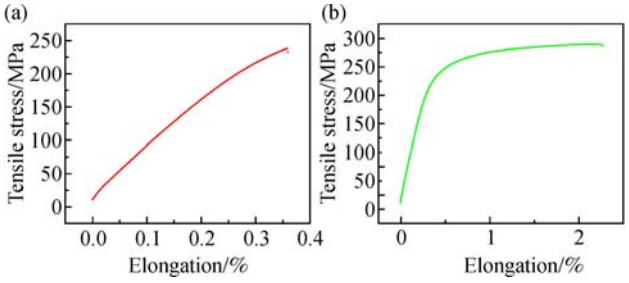

Fig. 4 Room temperature mechanical properties of (a) the first part produced by low-pressure die casting (Al-12Si-0.8Cu-0.5Fe-0.9Mg-0.7Ni-0.2Zn alloy) and (b) the second part produced by die casting (A356, Al-7Si-0.3Mg)

Figure 5 shows a 3D image of porosities (Fig. 5(a)) and a quantitative analysis of porosities (Fig. 5(b)) in the third part produced by SSC (A356, Al-7Si-0.3Mg). No significant porosity was observed. Careful examination revealed eight small porosities (Fig. 5(b)). The absence of porosity can be attributed to the typical solidification microstructure, as shown in Fig. 6.

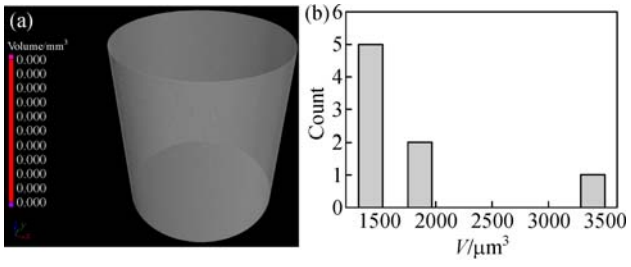

Fig. 5 (a) 3D image of porosities and (b) a quantitative analysis of porosities in the third part produced by semi-solid casting (A356, Al-7Si-0.3Mg)

Figure 6 shows an optical microscopy image (Fig. 6(a)) and a SEM image (Fig. 6(b)) of the third part produced by SSC (A356, Al-7Si-0.3Mg). As shown in Figs. 6(a) and 6(b), primary and secondary dendrites were broken, and round grains were formed. This result indicates that SSC could reduce the formation of porosities.

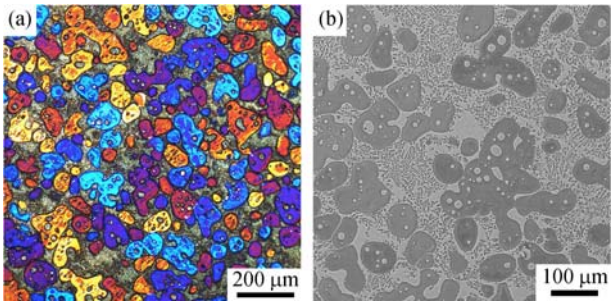

Fig. 6 (a) Optical microscopy image and (b) SEM image of the third part produced by SSC (A356, Al-7Si-0.3Mg)

4 Conclusions

Casting defects and eutectic grain boundaries in three types of near-net shape casting aluminum parts (LPDC Al-12Si-0.8Cu-0.5Fe-0.9Mg-0.7Ni-0.2Zn alloy; die casting A356, Al-7Si-0.3Mg; and SSC A356, Al-7Si-0.3Mg) were determined by CT. LPDC significantly reduced the formation of casting defects (i.e., porosity) due to its smooth filling and solidification under pressure. No significant casting defect was observed in the third part, indicating that SSC could produce high-quality near-net shape casting aluminum parts. Moreover, casting defects were mostly distributed along the eutectic grain boundaries, indicating that the refinement of eutectic grains is necessary to optimize the distribution of casting defects and decrease their size. This investigation revealed that CT is an efficient method to determine casting defects in near-net shape casting aluminum parts.

Acknowledgements Jiehua Li acknowledges the financial support provided by the Major International (Regional) Joint Research Project (Grant No. 51420105005) and Overseas, Hong Kong, Macao Scholars Cooperative Research Fund (Grant No. 51728101) from China.

References

1. Guo S J, Xu Y, Han Y, et al. Near net shape casting process for producing high strength 6xxx aluminum alloy automobile suspension parts. Transactions of Nonferrous Metals Society of China, 2014, 24(7): 2393–2400
2. Kamat G R. Low pressure counter gravity casting of aluminium alloys. Transactions of the Indian Institute of Metals (India), 1992, 45(3): 177–180
3. Chandley G D. Counter gravity casting of aluminum in investment and sand molds. American Foundrymen's Society, 1986, 94: 209–214
4. Jie W Q, Li X L, Hao Q T. Counter-gravity casting equipment and technologies for thin-walled Al-alloy parts in resin sand molds. Materials Science Forum, 2009, 618–619: 585–589

5. Chandley G D. Use of vacuum for counter-gravity casting of metals. Materials Research Innovations, 1999, 3(1): 14–23
6. Rosc J, Pabel T, Geier G F, et al. Method for the estimation of porosity analysis of CT-data. Giesserei-rundschau, 2010, 57: 244–246
7. Mayo S C, Stevenson A W, Wilkins S W. In-line phase-contrast X-ray imaging and tomography for materials science. Materials (Basel), 2012, 5(12): 937–965
8. Withers P J. Fracture mechanics by three-dimensional crack-tip synchrotron X-ray microscopy. Philosophical Transactions of the Royal Society A, 2015, 373(2036): 20130157
9. Samavedam S, Sakri S B, Hanumantha Rao D, et al. Estimation of porosity and shrinkage in a cast eutectic Al-Si alloy. Canadian Metallurgical Quarterly, 2014, 53(1): 55–64
10. Nicoletto G, Konečná R, Fintova S. Characterization of micro-shrinkage casting defects of Al-Si alloys by X-ray computed tomography and metallography. International Journal of Fatigue, 2012, 41: 39–46
11. Cabeza S, Mishurova T, Garcés G, et al. Stress-induced damage evolution in cast $AlSi_{12}CuMgNi$ alloy with one- and two-ceramic reinforcements. Journal of Materials Science, 2017, 52(17): 10198–10216